Processing and Application of Ceramics 16 [1] (2022) 78–82
https://doi.org/10.2298/PAC2201078S

The effect of alkaline earth metal substitution on thermoelectric properties of $A_{0.98}La_{0.02}MnO_{3-\delta}$ (A = Ca, Ba)

Sathya Prakash Singh[1], Nikola Kanas[1,2], Mari-Ann Einarsrud[1], Kjell Wiik[1,*]

[1]*Department of Materials Science and Engineering, NTNU Norwegian University of Science and Technology, 7491 Trondheim, Norway*

[2]*Present address: Institute BioSense, University of Novi Sad, 21000 Novi Sad, Serbia*

Received 14 December 2021; Received in revised form 27 January 2021; Accepted 14 February 2022

Abstract

The thermoelectric properties of ceramics with composition $A_{0.98}La_{0.02}MnO_{3-\delta}$ are anticipated to vary with the basicity and atomic portion of the alkaline earth metal, A. In the present investigation ceramic powder precursors with composition $A_{0.98}La_{0.02}MnO_{3-\delta}$ (A = Ca, Ba) were synthesized by the solid-state method and sintered in air at 1400 °C. Seebeck coefficient, electrical and thermal conductivities were characterized for both materials from 100 to 900 °C in air. The highest zT of 0.10 at 900 °C was reached for $Ca_{0.98}La_{0.02}MnO_{3-\delta}$. The high zT is attributed to the enhanced electronic conductivity (~90 S/cm at 900 °C) due to La doping. zT for $Ba_{0.98}La_{0.02}MnO_{3-\delta}$ reached its highest value (0.02) at 800 °C corresponding to a low electronic conductivity (~2 S/cm), while the thermal conductivity was significantly reduced compared to $Ca_{0.98}La_{0.02}MnO_{3-\delta}$ reaching ~1 W/(m·K) combined with a high Seebeck coefficient, −290 μV/K. The present data represent a valuable basis for further development of these materials with respect to applications in thermoelectric devices.

Keywords: *manganites, thermoelectric properties, alkaline earth metal ion substitution, tolerance factor*

I. Introduction

Thermoelectric generators (TEGs) are a combination of *n*- and *p*-type materials and possess the ability to convert heat directly into electrical energy by the Seebeck effect [1]. Integration of TEGs in high-temperature industrial processes will enhance the energy efficiency by waste heat harvesting and reduce the greenhouse gas emissions. The state-of-the-art *n*- and *p*-type thermoelectric materials (metals and alloys) are ruled out due to oxidation and melting at high temperatures in ambient air [2]. Thus, oxides become a relevant choice due to the stability in oxidizing atmosphere at high temperatures. However, oxides usually demonstrate low thermoelectric performance mainly due to the low electronic conductivity.

Whereas some *p*-type oxides possess good TE-performance [3], the *n*-type oxides demonstrate significantly lower performance [4–7]. The efficiency of thermoelectric materials is generally described by the dimensionless figure-of-merit [8]:

$$z \cdot T = \frac{\sigma \cdot S^2 \cdot T}{\kappa} \tag{1}$$

where σ, S and κ are electronic conductivity, Seebeck coefficient and thermal conductivity, respectively. According to Eq. 1, the figure-of-merit is enhanced by low thermal conductivity, high electronic conductivity and large Seebeck coefficient at high temperature.

Oxides with perovskite structure (ABO_3) are versatile in terms of A- and B-site doping, which enables tailoring of properties in a wide-range. $CaMnO_3$ (CMO) has perovskite structure and shows *n*-type electronic conductivity due to a polaron hopping mechanism. So far, the highest reported *zT* for CMO is 0.25 at 950 °C [9] and 0.32 at 800 °C [7] obtained by Nb and W doping, respectively. The electronic properties of CMO are governed by the electronic structure of Mn combined with the ratio between the oxidation states. The purpose of this study was to investigate the effect on TE-properties by replacing Ca with the larger alkaline earth element Ba. The ionic radii of 12-coordinated Ca^{2+} and Ba^{2+} are 0.134 and 0.161 nm, respectively [10].

* Corresponding author: tel: +47 73594082,
e-mail: *kjell.wiik@ntnu.no*

Since the basicity of Ba is higher than for Ca, it is anticipated that the oxidation state of the acidic Mn on B-site will increase with increasing basicity of the A-site element corresponding to an enhanced amount of oxygen (reduced δ) per formula unit [11]. In order to enhance the electronic conductivity, the materials were donor doped with La, and $Ca_{0.98}La_{0.02}MnO_{3-\delta}$ (2LCMO) and $Ba_{0.98}La_{0.02}MnO_{3-\delta}$ (2LBMO) were systematically characterized with respect to their TE properties. The effect of A-site substitution on the TE properties is discussed. To the best of our knowledge, a study of the effect of alkaline earth elements on TE-properties of $A_{0.98}La_{0.02}MnO_{3-\delta}$ (A = Ca, Ba) has not yet been reported.

II. Experimental procedure

The samples were synthesized by the solid-state reaction method (SSR) using $CaCO_3$, (99.99%, Merck), $BaCO_3$ (99.99%, Sigma Aldrich), La_2O_3 (99.99%, Sigma Aldrich) and MnO_2 (99.9%, Sigma Aldrich). Stoichiometric amounts of the dried precursors were mixed and planetary ball-milled (PM 100, Retsch) in isopropanol using YSZ-balls for 2 h followed by drying in a rotavapor (Butch Rotavapor) and pressing (100 MPa) to form pellets. All samples were heat-treated at 1200 °C for 6 h in reducing atmosphere (5% H_2/Ar), with heating and cooling rate of 200 °C/h. The obtained products were crushed in an agate mortar followed by wet planetary milling and drying. The green pellets (for thermal conductivity: 12.7 × 1.5 mm) and bars (for electrical conductivity and Seebeck measurements: 4 × 4 × 15 mm) were cold isostatically pressed (CIP) at 200 MPa followed by sintering at 1400 °C for 10 h in air. Heating rate of 200 and cooling rate of 60 °C/h were applied. The details and motivation for the two-step processing route are described elsewhere [12].

Bulk densities were determined by the Archimedes method in isopropanol. The bulk samples were finely ground and analysed by X-ray diffraction (XRD) (Bruker AXS D8-Advance X-ray diffractometer) using Cu Kα radiation and a LYNXEYE XE detector, with counting time 0.2 s in the range 10–75° (2θ angles) and 0.92 °/min scan rate.

DC-electrical conductivity measurements were performed by the four-probe method (In-house built setup [13,14]) using Pt electrodes. The distance between the Pt-voltage probes in the set up was 5.0 mm while the current Pt-probes were positioned at each end of the sample. Seebeck coefficient measurements were done by a Probostat™ (NORecS) in a vertical furnace where a temperature gradient in the range between 4 and 7 K was generated along the sample. The generated Seebeck voltage was measured via Pt-electrodes. The thermal conductivity was measured by the laser flash method (Netzsch LFA 457 MicroFlash) on disc shaped samples (D = 12.2 mm). All the TE measurements were performed in synthetic air up to 900 °C with increments of 100 °C.

III. Results and discussion

3.1. Characteristics of bulk ceramics

XRD patterns presented in Fig. 1 show that the bulk 2LCMO and 2LBMO samples are single-phase materials, with orthorhombic and hexagonal structure, respectively. According to the calculated tolerance factor values (Table S1, Supplementary data[§]) there is a good agreement between the predicted and observed structures.

The relative densities of 2LCMO and 2LBMO samples were 87 and 76 %TD, respectively (Table S2). The bulk densities indicate that the densification of hexagonal perovskite like structures (face sharing octahedral units) is more challenging compared to perovskite like structures with corner-sharing octahedral units.

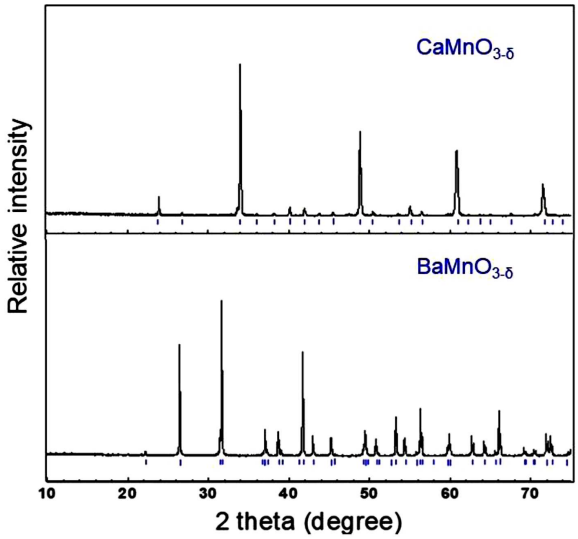

Figure 1. XRD patterns of 2LCMO (PDF 01-014-8192) and 2LBMO (PDF 04-014-7311) bulk ceramics

3.2. Thermoelectric properties

The effect of donor doping in $AMnO_{3-\delta}$ is illustrated by Eq. 2 (using the Kroeger-Vink notation):

$$0.5\,La_2O_3 \xrightarrow{AMnO_{3-\delta}} La_A^{\bullet} + e' + 1.5\,O_O^x \qquad (2)$$

where A is Ca or Ba, $La_A^{\bullet}$ is trivalent La on divalent A-site, e' is electron and O_O^x is oxygen on oxygen site. According to Eq. 2 the concentration of electrons will increase with increasing substitution level, corresponding to enhanced electronic conductivity.

The electrical conductivities of both ceramics are presented in Fig. 2a as a function of temperature. The electronic conductivity of 2LCMO ceramics increases exponentially with temperature reaching about 90 S/cm, whereas 2LBMO sample demonstrates significantly lower and relatively constant values in the same temperature range. The variations in electronic conductivity with temperature for undoped CMO and BMO, based on the literature data [9,15,16], are given

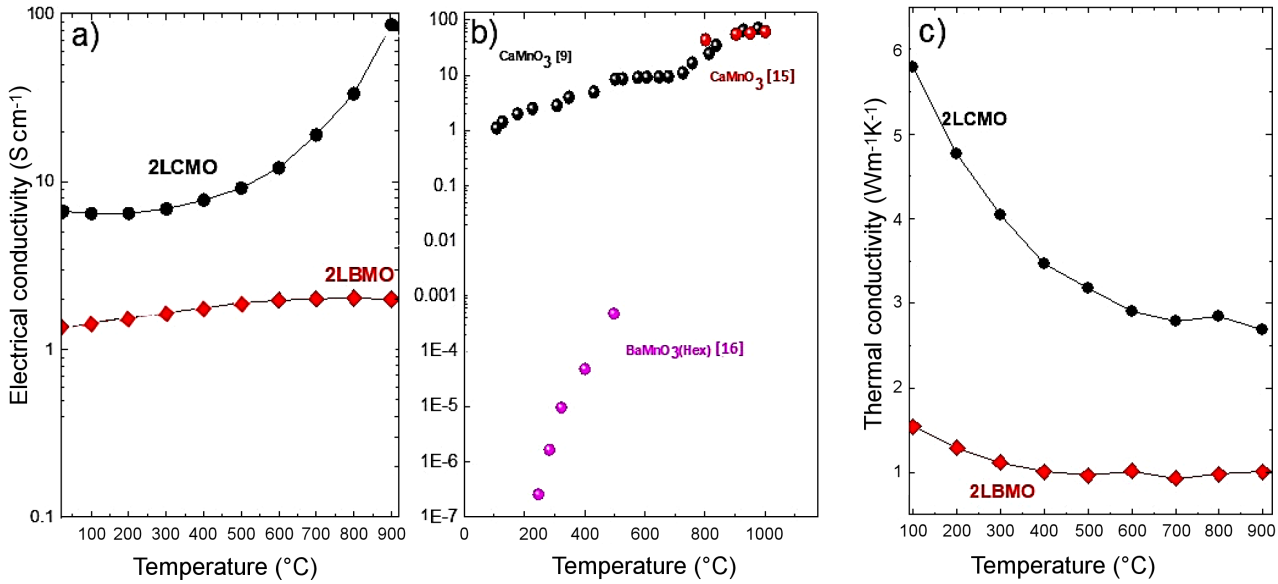

Figure 2. Electrical conductivity as a function of temperature for: a) 2LCMO and 2LBMO, b) un-doped CMO [9,15] and BMO ceramics [16] and c) thermal conductivity as a function of temperature for 2LCMO and 2LBMO ceramics

in Fig. 2b. Comparing the electronic conductivity data of 2LBMO with the pure BMO, it is obvious that La enhances the conductivity with many orders of magnitude. At $T < 800\,°C$, 2LCMO ceramics also shows enhanced electronic conductivity compared with the undoped CMO. However, at even higher temperatures 2LCMO ceramics shows similar conductivities as reported by Thiel *et al*. [9] and Schrade *et al*. [15] as well as the undoped compositions. This is in correspondence with a polaron hopping conductivity mechanism at high temperatures and was thoroughly discussed by Franchini *et al*. [17].

The reduction in electronic conductivity by replacing Ca with Ba is significant (Fig. 2a) and could not be explained by the lower bulk density of 2LBMO compared to 2LCMO sample. At conditions where polaron hopping is not dominant (medium and low temperatures) it is anticipated that the reduced electronic conductivity of 2LBMO sample is due to the large Ba-ion giving less overlap between the atomic orbitals of the Mn–O–Mn bridge which represents the pathway for electrons [16]. At higher temperatures it is expected that polaron hopping will be activated followed by a significant increase in electronic conductivity as it is observed for 2LCMO sample. However, the polaron mechanism depends on the ratio between $[Mn^{3+}]$ and $[Mn^{4+}]$ and electrons hopping between these sites [15]. Due to the high basicity of Ba compared to Ca it is reasonable to assume that the acidic Mn-ion is oxidized to Mn^{4+} [11] and the remaining low concentration of Mn^{3+} will reduce the electronic conductivity due to polaron hopping significantly in accordance with the observations reported in Fig. 2a. It also acknowledged that there is some variation in both density and grain size between 2LCMO and 2LBMO ceramics (Table S2), and that high density and large grains in general are beneficial for the electrical conductivity.

The importance of a low thermal conductivity to reach a high figure-of-merit is obvious from Eq. 1. The total thermal conductivity, κ_t, can be written as $\kappa_t = \kappa_l + \kappa_e$ where κ_l is lattice contribution, due to phonons, and κ_e is the electronic contribution. The decrease in the κ_l with increasing temperature is due to the dominance of phonon-phonon scattering and at high electronic conductivities the contribution from κ_e will become significant (e.g. metals). Phonon scattering will increase both with decreasing grain size (scattering at grain boundaries) and increasing atomic number. At low and medium temperatures, the thermal conductivity will also decrease with increasing porosity. The thermal conductivity of the two materials is presented in Fig. 2c and it is evident that 2LCMO shows significantly higher thermal conductivity than 2LBMO sample. The enhanced κ is due to the higher density (low porosity) and the lower atomic mass of Ca compared to Ba as well as the large grains in 2LCMO sample (Table S2). Although the electronic conductivity of 2LCMO is much higher than for 2LBMO ceramics, the contribution from electrons is rather modest corresponding to 7% of κ_t at 900 °C, calculated according to the Wiedemann-Franz Law [19]. Significantly lower thermal conductivity is observed for 2LBMO, reaching values below 1 W/(m·K) at $T > 400\,°C$. It is assumed that this is due to a high concentration of Ba combined with a high porosity and enhanced phonon scattering at grain boundaries due to small grains (Table S2).

Seebeck coefficients, S, for 2LCMO and 2LBMO ceramics are given in Fig. 3a and confirm the n-type nature of both materials. The simplest approach to assess S is given by the classical relationship between S and the concentration of charge carriers, n [18]:

$$S = \frac{8\pi^2 \cdot \kappa_{B^2}}{3e \cdot h^2} m^* \cdot T \left(\frac{\pi}{3n}\right)^{\frac{2}{3}} \tag{3}$$

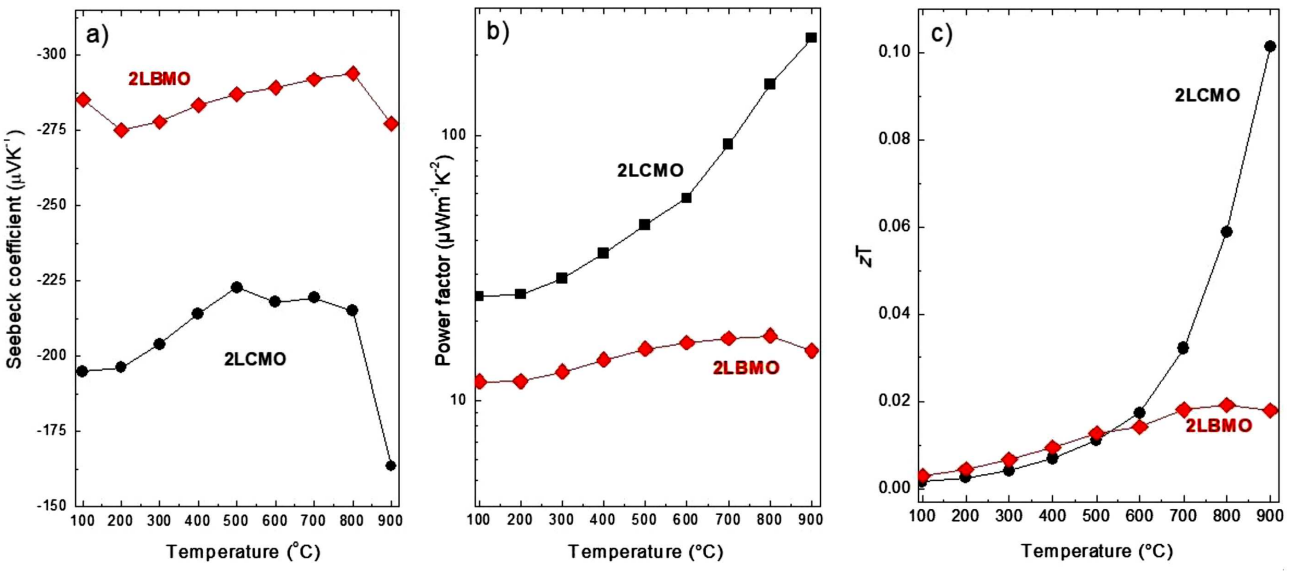

Figure 3. Temperature dependence of a) Seebeck coefficient, b) power factor and c) zT of 2LCMO and 2LBMO in air

where κ_B is the Boltzmann constant, e is the elementary charge, h is Plank's constant, m^* is the effective mass of charge carrier and T is the absolute temperature. According to Eq. 3, $|S|$ will be proportional to the carrier concentration, $n^{-2/3}$, at a given temperature T. Comparing the individual materials, the lower $|S|$ of 2LCMO sample is attributed to the higher electronic conductivity. The significant reduction in Seebeck coefficient for 2LCMO ceramics from 800 to 900 °C also supports the explanation that the charge carrier concentration and polaron hopping mechanism is dominant at high temperatures. The highest $|S|$ of 290 μV/K at 800 °C is obtained with 2LBMO in accordance with the low electronic conductivity. It should also be noted that there is a minor reduction in S also for LBMO ceramics at $T > 800$ °C, which is not correlated with σ in Fig. 2a. The reason for the discrepancy is left unexplained but may be related to deviation from the simplified assumption that there is a direct proportionality between σ and n, since variation in the mobility of charged species also plays a role. The power factor, P, is the product between electrical conductivity and Seebeck coefficient squared ($P = S \cdot \sigma^2$) and is presented in Fig. 3b. Comparing S (Fig. 3a) and σ (Fig. 2a) it is seen that P is governed by the electrical conductivity. 2LCMO shows a significantly higher P than 2LBMO ceramics at all temperatures, reaching about 210 μW/m·K^2 at 900 °C, which is higher than previously reported by Singh *et al.* [12] and comparable to Bocher *et al.* [7]. In applications such as electric power generation by thermoelectric devices, P is one of the most important parameters [20,21].

The figure-of-merit (zT) as a function of temperature is given in Fig. 3c. At $T < 600$ °C both materials show rather moderate zT values, however somewhat higher values are observed for 2LBMO ceramics due to its low thermal conductivity (Fig. 2c). At $T > 600$ °C there is a notable enhancement in zT for 2LCMO ceramics, showing the significance of electrical conductivity which shows a substantial increase at temperatures above 600 °C (Fig. 2a).

Hence, among the two materials investigated, 2LCMO shows promising properties with respect to high temperature applications in TE-devices.

However, a further optimization of the TE properties is needed, and a viable route is to enhance the electronic conductivity by further optimized doping (and co-doping) combined with "grain-engineering" at the nanoscale to reduce the thermal conductivity. It is also interesting to notice the low thermal conductivity of 2LBMO ceramics (Fig. 2c) and given that electronic conductivity may be enhanced by proper doping, this material system would also be worth a further study.

IV. Conclusions

Bulk $A_{0.98}La_{0.02}MnO_{3-\delta}$ (A = Ca, Ba) ceramics were successfully fabricated by the solid-state method in reducing atmosphere, followed by sintering in synthetic air. The best performance at high temperatures in terms of zT was obtained for $Ca_{0.98}La_{0.02}MnO_{3-\delta}$, reaching a maximum of about 0.10 at 900 °C attributed to high electronic conductivity. A further study of donor doped $Ca_{0.98}La_{0.02}MnO_{3-\delta}$ is proposed aiming at both a further increase in the electronic conductivity by appropriate doping/co-doping and a reduction in the thermal conductivity by grain boundary engineering at the nano-range. $Ba_{0.98}La_{0.02}MnO_{3-\delta}$ ceramics reached a zT of less than 0.02 at high temperatures due to a low electronic conductivity. The low electronic conductivity is explained by the enhanced basicity of Ba compared with Ca, shifting the oxidation state of manganese to Mn^{4+}. The thermal conductivity of $Ba_{0.98}La_{0.02}MnO_{3-\delta}$ sample was encouragingly low (~1 W/(m·K) at $T > 400$ °C) combined with a high Seebeck coefficient (−290 μV/K at 800 °C), and a further study aimed at enhancing the electronic conductivity by appropriate doping/co-doping is recommended.

Acknowledgements: Financial support from The Research Council of Norway under the program Nano2021: "Thermoelectric materials: Nanostructuring for improving the energy efficiency of thermoelectric generators and heat-pumps" (THELMA, Project no.: 228854) and the Antares program (Grant ID: 739570) is gratefully acknowledged.

§ Supplementary data can be downloaded using following link: https://bit.ly/34V8zYp

References

1. S. Walia, S. Balendhran, H. Nili, S. Zhuiykov, G. Rosengarten, Q.H. Wange, M. Bhaskaran, S. Sriram, M.S. Strano, K.K. Zadeh, "Transition metal oxides – Thermoelectric properties", *Prog. Mater. Sci.*, **58** (2013) 1443–1489.
2. W. Xie, X. Tang, Y. Yan, Q. Zhang, T.M. Tritt, "High thermoelectric performance BiSbTe alloy with unique low-dimensional structure", *J. Appl. Phys*., **105** (2009) 113713.
3. K. Koumoto, I. Terasaki, R. Funahashi, "Complex oxide materials for potential thermoelectric applications", *MRS Bull.*, **31** (2011) 206–210.
4. M. Ohtaki, K. Araki, K. Yamamoto, "High thermoelectric performance of dually doped ZnO ceramics", *J. Electron. Mater.*, **38** (2009) 1234–1238.
5. T. Tsubota, M. Ohtaki, K. Eguchi, H. Arai, "Thermoelectric properties of Al-doped ZnO as a promising oxide material for high-temperature thermoelectric conversion", *J. Mater. Chem.*, **7** (1997) 85–90.
6. Z. Lu, H. Zhang, W. Lei, D.C. Sinclair, I.M. Reaney, "High-figure-of-merit thermoelectric La-doped A-site-deficient $SrTiO_3$ ceramics", *Chem. Mater.*, **28** (2016) 925–935.
7. L. Bocher, M.H. Aguierre, D. Logvinovich, A. Shkabko, R. Robert, M. Trottman, A. Weidenkaff, "$CaMn_{1-x}Nb_xO_3$ ($x \leq 0.08$) perovskite-type phases as promising new high-temperature n-type thermoelectric materials", *Inorg. Chem*., **47** (2008) 8077–8085.
8. A.F. Ioffe, *Semiconductor Thermoelements and Thermoelectric Cooling.* Translated from Russian, Infosearch Ltd, London, 1957.
9. P. Thiel, J. Eilertsen, S. Populoh, G. Saucke, M. Döbeli, A. Shkabko, L. Sagarna, L. Karvonen, A. Weidenkaff, "Influence of tungsten substitution and oxygen deficiency on the thermoelectric properties of $CaMnO_{3-\delta}$", *J. Appl. Phys.*, **114** (2013) 243707.
10. R.D. Shannon, "Revised effective ionic radii and systematic studies of interatomie distances in halides and chaleogenides", *Acta Cryst.*, **A32** (1976) 751–767.
11. F.G.K. Baucke, J.A. Duffy, "The effect of basicity on redox equilibria in molten glasses", *Phys. Chem.Glasses*, **32** (1991) 211–218.
12. S.P. Singh, N. Kanas, T.D. Desissa, M.-A. Einarsrud, T. Norby, K. Wiik, "Thermoelectric properties of non-stoichiometric $CaMnO_{3-\delta}$ composites formed by redox-activated exsolution", *J. Eur. Ceram. Soc.*, **40** (2020) 1344–1351.
13. N. Kanas, S.P. Singh, M. Rotan, M. Saleemi, M. Bittner, A. Feldhoff, T. Norby, K. Wiik, T. Grande, M.-A. Einarsrud, "Influence of processing on stability, microstructure and thermoelectric properties of $Ca_3Co_{4-x}O_{9+\delta}$", *J. Eur. Ceram. Soc.,* **38** (2018) 1592–1599.
14. I. Waernhus, *Defect chemistry, conductivity and mass transport properties of $La_{1-x}Sr_xFeO_3$ (x=0 and 0.1)*, PhD thesis, Depart. Mater. Sci. Eng., Norwegian University of Science and Technology, Trondheim, Norway, 2003.
15. M. Schrade, R. Kabir, S. Li, T. Norby, T. Finstad, "High temperature transport properties of thermoelectric $CaMnO_{3-\delta}$ - Indication of strongly interacting small polarons", *J. Appl. Phys.*, **115** (2014) 103705.
16. E. Markiewicz, R. Bujakiewicz-Koronska, A. Budziak, A. Kalvane, D.M. Nalecz, "Impedance spectroscopy studies of $SrMnO_3$, $BaMnO_3$ and $Ba_{0.5}Sr_{0.5}MnO_3$ ceramics", *Phase Transit.*, **87** (2014) 1060–1072.
17. C. Franchini, M. Reticcioli, M. Setvin, U. Diebold, "Polarons in materials", *Nat. Rev. Mater*., **6** (2021) 560–586.
18. S.G. Jeffrey, E.S. Toberer, "Complex thermoelectric materials", *Nat Mater.,* **7** (2008) 105–114.
19. N. Kanas, S.P. Singh, M. Rotan, T.D. Desissa, T. Norby, K. Wiik, T. Grande, M.-A. Einarsrud, "Thermoelectric properties of $Ca_3Co_{2-x}Mn_xO_6$ (x = 0.05, 0.2, 0.5, 0.75, and 1)", *Materials,* **12** (2019) 497–507.
20. D. Narducci, "Do we really need high thermoelectric figure of merit, A critical appraisal to the power conversion efficiency of thermoelectric materials", *Appl. Phys. Lett*., **99** (2011) 102104.
21. M. Bittner, N. Kanas, R. Hinterding, F. Steinbach, J. Rathel, M. Schrade, K. Wiik, M.-A. Einarsrud, A. Feldhoff, "A comprehensive study on improved power materials for high-temperature thermoelectric generators", *J. Power Sources*., **410** (2019) 143–151.
22. S.G. Jeffrey, E.S. Toberer, "Complex thermoelectric materials", *Nat. Mater.,* **7** (2008) 105–114.